AIAA JOURNAL
Vol. 36, No. 4, April 1998

# Effects of Periodic Excitation on Turbulent Flow Separation from a Flap

B. Nishri* and I. Wygnanski†
*Tel-Aviv University, Ramat-Aviv 69978, Israel*

**The effects of periodic perturbations on delaying separation or promoting reattachment of initially separated flow were experimentally investigated. The leading parameters affecting the flow are the flap deflection, the input momentum, and its reduced frequency. The sensitivity of the flow to the imposed oscillations depends on its initial state, and this leads to hysteresis with respect to changes in any of the aforementioned parameters. For example, the most effective frequency required to attach the flow to the surface is much lower than the one required to prevent its separation. The amplitude needed to force reattachment may be an order of magnitude larger than the amplitude required to prevent separation at a given inclination of the flap. Nevertheless, periodic forcing is much more effective than steady blowing for boundary-layer control.**

## Nomenclature

$C_p$ = pressure coefficient, $(p - p_i)/q$
$C_\mu$ = combined momentum coefficient, $\equiv(c_\mu; \langle c_\mu \rangle)$
$c_{mh}$ = hinge moment on a flap
$c_n$ = normal force on a flap
$c_\mu$ = steady blowing momentum coefficient, $\equiv(J/q \times L) = 2(g/L) \times [U_j/U_i]^2$
$\langle c_\mu \rangle$ = oscillatory momentum coefficient, $\equiv 2(g/L) \times [\langle u' \rangle_f / U_i]^2$
$F^+$ = dimensionless frequency, $\equiv(f \times L)/U_i$
$f$ = predominant frequency of the imposed oscillations
$G$ = step height at the trailing edge of the splitter plate
$g$ = gap between the trailing edge of the splitter plate and the flap
$H$ = boundary-layer shape factor, $\delta^*/\theta$
$J$ = mean jet momentum near the slot, $\equiv \rho U_j^2 g$
$\langle J \rangle$ = phase-locked oscillatory momentum near the actuator, $\equiv \rho \int_0^\infty \langle u' \rangle_f^2 \, dy$
$L_f$ = flap length
$q$ = freestream dynamic pressure, $\frac{1}{2}\rho U_i^2$
$Re_L$ = flap Reynolds number, $U_i L/\nu$
$U_i$ = freestream reference velocity
$U_j$ = average exit velocity of the slot, $\int_0^\infty U_J \, dy$
$U_\chi$ = phase velocity
$u'$ = rms of the streamwise component of the velocity fluctuations
$\langle u' \rangle_f$ = phase-locked rms amplitude of the velocity at the forcing frequency
$x$ = distance along the flap
$x_{cp}$ = center of pressure location, $c_{mh}/c_n$
$y$ = distance normal to the flap
$\alpha$ = flap deflection angle
$\delta^*$ = boundary-layer displacement thickness
$\theta$ = boundary-layer momentum thickness
$\nu$ = kinematic viscosity
$\rho$ = density

*Subscripts*

$i$ = reference location far upstream
$r$ = conditions at reattachment with forcing
$r_0$ = conditions at naturally reattached flow
$s$ = conditions at separation with forcing
$s_0$ = conditions at natural separation
$\infty$ = local freestream conditions

Received Jan. 31, 1997; revision received Aug. 10, 1997; accepted for publication Oct. 15, 1997. 

*Research Associate, Faculty of Engineering.
†Professor, Faculty of Engineering; also Professor, Department of Aerospace Engineering, University of Arizona, Tucson, AZ 85721. Fellow AIAA.

## I. Introduction

PERIODIC perturbations introduced at the knee of a highly deflected flap (Fig. 1) are very effective in delaying or reversing the separation over the flap,[1,2] because they evolve into large eddies transporting momentum from the freestream to the surface. Whenever these perturbations are introduced after the occurrence of separation, they have to be large enough and robust enough to span the recirculating zone and transport momentum across it (Fig. 2). This, in turn, forces the flow to resume its original direction and appear as a regular, thick boundary layer in the mean.[1] Thus the addition of periodic motion enables the flow to withstand or to generate more severe adverse pressure gradients than otherwise possible. It enhances the lift and reduces the drag of airfoils,[3,4] enabling them to be thicker or more inclined to the oncoming flow; it also increases the effectiveness of diffusers by enabling them to be shorter without the concomitant loss of mean kinetic energy.

When separation is to be prevented at large flap deflections, active flow control should overcome all known indicators of impending separation, such as excessive bubble dimensions, boundary-layer momentum thickness, or shape factor. Steady tangential blowing provides excess momentum (changing at times the sign of the resulting momentum thickness) but relies on entrainment for its redistribution across the flow. When the flow is detached from the surface, a mixing layer is formed between a constant velocity stream above it and the dead-water region adjacent to the surface. The mean streamlines in the freestream do not curve or diverge, indicating a total loss of the reaction force and pressure recovery. Thus the goal in this case is to generate a pressure difference across the mixing layer, forcing it toward the surface. The most obvious way to attain it is by bringing the surface closer to the mixing layer, thereby limiting the total mass of fluid available for entrainment on its low-velocity side. One may also achieve a similar result by enhancing the entrainment rate of the mixing layer from the limited reservoir of fluid bound by it and by the solid surface. The downward momentum generated by the reattachment creates a reaction force normal to the surface of the flap. The flow resulting from forced reattachment may differ from the flow prevailing before separation. Thus, the procedure used to deflect the flow is only a first step in a control strategy whose purpose is to get the largest possible deflection of the surface using the smallest momentum input.

A large number of parameters govern the control of separation over a complex airfoil. Therefore, this study endeavors to determine the significance of each parameter. The detachment of the flow over a straight flap can be controlled easily because it is simple, there is no curvature involved, it is sensitive to small changes in pressure gradient, and it has a well-defined location of separation. By

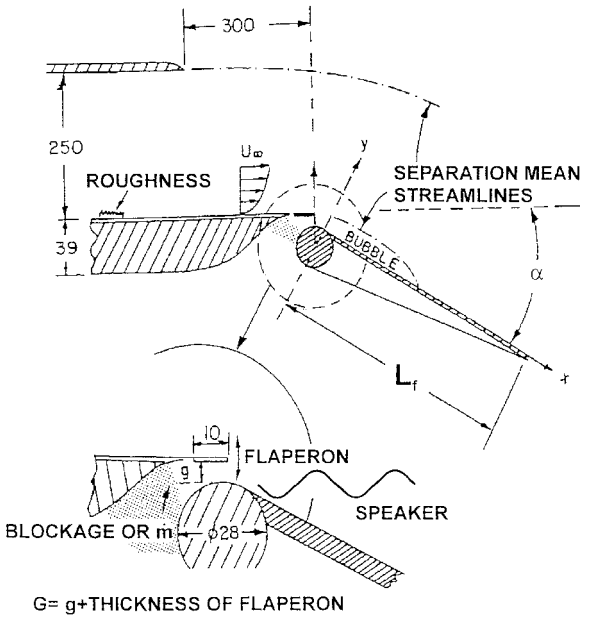


**Fig. 1 Sketch of the flap and the region around the flap shoulder.**

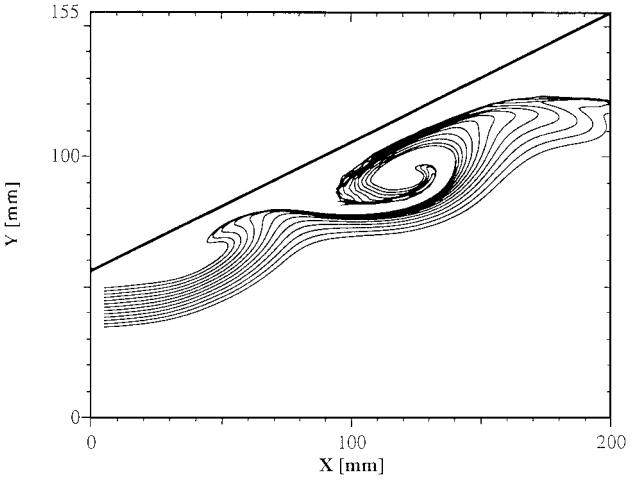


**Fig. 2 Reconstructed streakline pattern showing a forced flow over the flap: $F^+ = 1.2$, $L_f = 200$ mm, and $Re = 165 \times 10^3$ (courtesy of A. Darabi).**

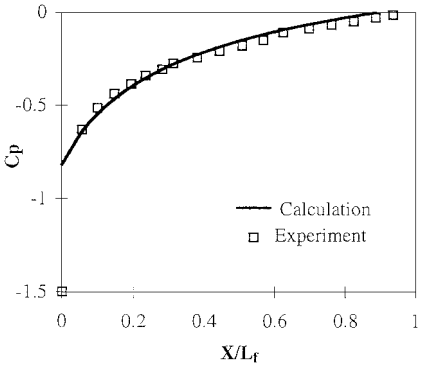


**Fig. 3 Comparison between the measured and calculated pressure distributions over the flap at small angles of inclination: $F^+ = 0$, $\alpha = 24$ deg, $C_\mu = 0$, and $G = 1.5$ mm.**

increasing the deflection angle (Fig. 1), the ideal adverse pressure gradient negotiated by the flow increases until the flow separates. At small angles of deflection a bubble, which grows rapidly with increasing $\alpha$, is formed, leading to a complete detachment of the flow when a threshold in $\alpha$ is surpassed. Special attention was paid to optimize the parameters delaying separation or enhancing reattachment of separated flow.

## II. Experiment and Data Acquisition

A schematic drawing of the generic flap experiment is provided (Fig. 1), and a detailed description of the apparatus and calibration procedures is given in Ref. 2. The floor of a cascade wind tunnel was used to impose the adverse pressure gradient while the presence or absence of the tunnel ceiling determined whether the simulated flow represented a two-dimensional diffuser or a trailing-edge flap. In this experiment the entire stream was deflected, representing the flow over a flap. Boundary-layer coordinates were used, and the traverse mechanism was inclined accordingly. The turbulent boundary layer approaching the trailing edge of the upstream plate was carefully documented across the entire span. Coarse, randomly distributed roughness was placed on this plate to trip and to thicken the upstream boundary layer and to assess its effect on the ensuing flow on the flap. The mean flow is two dimensional, and the velocity profiles are typical of a turbulent boundary layer having a shape factor $H = 1.46$. The Reynolds number based on the reference momentum thickness $\theta_i$ varied from $10^3$ to $8 \times 10^3$.

The imposed phase-locked velocity perturbations were measured very close to the actuator (or the slot) and were expressed in terms of $\langle c_\mu \rangle$. An identical calibration procedure was used for periodic blowing on airfoils.[1,4] The procedure was repeated not only for a variety of inputs (frequencies and amplitudes) but also for a variety of upstream (for different boundary-layer thickness) and downstream (separated or attached) flow conditions. This provided the ability to maintain constant amplitude at various frequencies and flow conditions whenever required. The oscillatory component of the jet momentum is based on its rms value; thus, in the presence of steady blowing, the total momentum coefficient is given by the sum $C_\mu = [c_\mu + \langle c_\mu \rangle]$ as defined in Ref. 4.

## III. Dimensional Analysis of the Flow

The leading independent parameters governing the flow over the deflected flap in the absence of steady blowing, $U_j$, are $\alpha$, $L_f$, $G$, $x$, $\delta_i^*$, $U_i$, $f$, $\langle u_j' \rangle$, $\nu$, and $\rho$. The dependent parameters of interest are the pressure distribution along the flap, the characteristics of the boundary layer or the mixing layer over it when the flow is either partially or entirely separated, and the resulting forces and moments on it. The local $c_p$ or $\delta^*$ depends on the following dimensionless parameters:

$$\delta^* = \delta^*\left[\Delta\,\alpha,\, F^+,\, Re,\, x/L_f,\, G/L_f,\, \delta_i^*/L_f,\, \langle c_\mu \rangle\right] \qquad (1)$$

where $\Delta\,\alpha$ refers to deflection angles in excess of those at which separation or reattachment occurs naturally, i.e., $\Delta\,\alpha_s = (\alpha - \alpha_{s0})$ and $\Delta\,\alpha_r = (\alpha - \alpha_{r0})$.

In this way the initial condition of the flow is accounted for because the flap deflection $\alpha$ is either referred to $\alpha_{s0}$ or to $\alpha_{r0}$. The number of independent parameters is further reduced in the absence of external control because $F^+$ and $\langle c_\mu \rangle$ drop out. The geometry considered may resemble the classical corner flow, provided the total height of the step $G$ and the upstream boundary-layer thickness $\delta_i^*$ are vanishingly small, i.e., $G/x \ll 1$ and $\delta_i^*/x \ll 1$ in the range of $x$ distances of interest. In this case, $c_p = c_p[\alpha, Re, x/L_f]$, which tends to be independent of viscosity at high Reynolds numbers and may, at large values of $x$, be approximated by the ideal flow solution

$$c_p = 1 - (U/U_i)^2 = 1 - X^{[-2\alpha/(\pi+\alpha)]} \qquad (2)$$

where $X = (x - x_0)/L_f$, and $x_0$ represents the location of the virtual origin. The use of $x_0$ is necessary to account for the bubble located near the leading edge of the flap and for its finite length.

The agreement between the $c_p$ predicted and measured is good (Fig. 3), provided that one excludes the pressure coefficients measured near the bubble. The relative length of the virtual origin $x_0/L_f$ used for the comparison increases with increasing $\alpha$ because the length of the bubble increases as well. The potential flow solution provides the leading terms in the hierarchy considered. Thus, the most significant parameters affecting the control of separation or reattachment by periodic excitation are

$$c_p = c_p\left[\alpha,\, x/L_f,\, F^+,\, \langle c_\mu \rangle\right] \qquad (3)$$

as long as the discontinuities at the flap leading edge and the upstream boundary-layer thickness are not large. The first three parameters represent a ratio of length scales, where the length of the flap $L_f$ is chosen as the primary independent length, i.e., $\alpha = \sin^{-1}(h/L_f)$, where $h$ is the vertical distance of the trailing edge of the flap relative to the upstream surface, and $F^+ = L_f/\lambda$, where $\lambda$ is the wave length of the harmonic perturbation, $\lambda \propto U_i/f$. The choice of $L_f$ in the definition of $F^+$ is justified only when the perturbations are introduced at the leading edge of the flap; otherwise $L_f$ should be replaced by the distance between the actuator (or slot through which the perturbations are introduced) and the trailing edge of the flap. This point was proven while active control was used on airfoils.[4] The effects of viscosity may be discarded at high Reynolds numbers and reasonably high frequencies, making the viscous length scale $(\nu/f)^{1/2}$ insignificant. These limitations are of no concern in most aeronautical applications. The fourth parameter represents the amplitude of excitation in terms of the momentum added to the flow. It is analogous to a steady momentum coefficient $c_\mu$ so widely used in association with blowing. Thus, the effectiveness of this type of boundary-layer control can best be shown by comparing it with steady blowing where the combined momentum coefficient $C_\mu = (c_\mu + \langle c_\mu \rangle)$ is the controlling parameter.

The minimum $C_\mu$ required for maintaining attached flow or, alternately, for causing reattachment of separated flow at a prescribed $\alpha$ depends on $F^+$, whose magnitude can be estimated by simple reasoning. Consider a fully separated flow over a deflected flap at $\alpha = 30$ deg. In this case, the freestream is parallel to the upstream surface. The flow might reattach to the flap when the large eddies in the mixing layer come in contact with the trailing edge of the flap because then the entrainment into the mixing layer will pump out the fluid trapped between it and the flap. Consequently, the scale of the large eddies $\lambda$ should be commensurate with $h$, i.e., $\lambda \approx L_f \sin\alpha$. Because the phase velocity in a classical mixing layer between a steady stream and quiescent surrounding fluid is approximately $U_\chi \approx \frac{1}{2}U_\infty$, $F^+ = fL_f/U_\infty = [(U_\chi/\lambda)L_f/U_\infty] = (U_\chi/U_\infty)/(\lambda/L_f) \approx 1$. Another estimate of the most effective $F^+$ may be derived from experiments aimed at controlling the mixing layer. It was shown that perturbations introduced at the origin of the layer were amplified as long as $(fx/U_\infty) \leq 1$ (Refs. 5–7). Thus maximum amplitudes are attained at $x = L_f$ when $F^+ \approx 1$.

Upon reattachment, the flow contains a large bubble whose dimensions are commensurate with, but smaller than, the length of the flap. It can be maintained as long as the excitation $\langle c_\mu \rangle$ provides a sufficient margin of safety to prevent the recurrence of separation. Because the flow bounding the bubble is the familiar mixing layer[8] (at least over the initial 50% of its length, which is known for having a constant pressure), an increase in the excitation frequency will shorten the distance $x$ over which the imposed perturbations amplify, and it will hasten their rate of amplification. This, in turn, will further reduce the size of the bubble. There must be a limit to this procedure because the amplitudes imposed will decay over ever-increasing distances between the reattachment location and the trailing edge of the flap. A separation is bound to recur when the local amplitude of the oscillations transferring momentum from the outer stream to the surface falls below a threshold level required for that deflection (provided $\alpha > \alpha_{s_0}$). Such separation will presumably recur near the trailing edge where the anticipated amplitudes of the imposed high-frequency oscillations were dissipated most.

## IV. Results

### A. Some Features of the Base Flow over the Deflected Flap

The mean distributions of pressure on the surface of the deflected flap in the absence of externally imposed oscillations are plotted in Fig. 4 for a variety of flap deflections starting, with attached flow, at $\alpha = 20$ deg and ending with separation at $\alpha = 30.5$ deg. The total height of the step at the flap leading edge was maintained at $G = 0.006L_f$ (Fig. 1), and no flow was allowed through the slot, which was attached to a sealed plenum chamber or blocked by an insert. The extent of the negative pressure region increased with increasing $\alpha$ because the streamline leaving the trailing edge of the upstream surface reattached, enclosing a bubble whose length increased with increasing $\alpha$, until the flow separated around $\alpha = 30$ deg. The size of the bubble could not be estimated from pressure distributions; thus other criteria were established with the aid of hot wires, linking the mean location of reattachment $X_b$ with the most easily observed feature in the mean pressure distributions, i.e., the location at which $(\partial^2 p/\partial x^2) \equiv p'' = 0$ to give $0.45 \leq (X_{p''=0}/X_b) \leq 0.50$. The $x$ location at which $p'' = 0$ is pointed out in Fig. 4. The length of the bubble, according to this criterion, is almost proportional to $\alpha$ provided $\alpha > 24$ deg. At this angle $X_b > 0.45L_f$, and it becomes $0.96L_f$ before complete separation. The size of the bubble depends on $\alpha$, $L_f$, and $G$ and on the thickness of the upstream boundary layer. The streamwise distribution of $c_p$ was insensitive to the changes in Reynolds number. At $\alpha = 30.5$ deg the flow separated and the low-pressure region generated by the bubble collapsed. The variation of the bubble length with $\alpha$ was gradual and reversible, but the burst of the bubble was abrupt and irreversible. The detached flow was unaffected by small decreases in $\alpha$; it eventually reattached, quite abruptly as well, when $\alpha$ was reduced to approximately 25 deg.

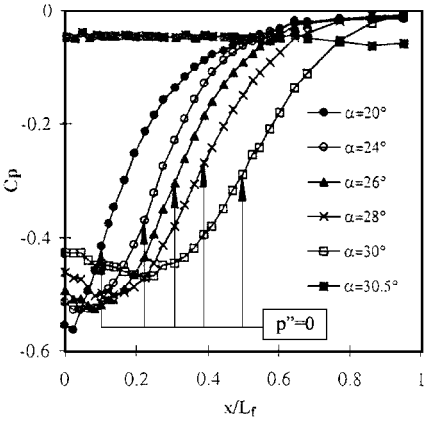


**Fig. 4 Dependence of the pressure distributions over the flap on the angles of inclination: $F^+ = 0$, $Re = 450 \times 10^3$, $L_f = 740$ mm, and $G/L_f = 0.6\%$.**

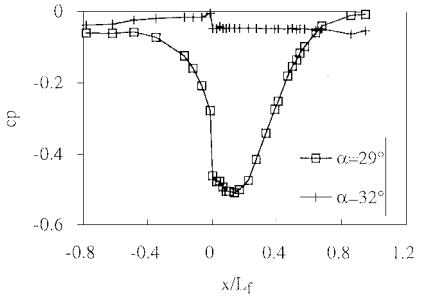


**Fig. 5 Upstream effect of separation on the pressure distribution: $F^+ = 0$, $Re = 450 \times 10^3$, $L_f = 740$ mm, $G/L_f = 0.6\%$, and $\alpha_{s_0} = 30.5$ deg.**

Pressure distributions showing the upstream effect of the flap deflection are plotted in Fig. 5. The distance $x$ is measured along the surface relative to the discontinuity ($x > 0$ is on the flap, whereas $x < 0$ is on the upstream surface). The data presented were measured at $\alpha = \alpha_{s_0} \pm 1.5$ deg; thus in one case the flow was separated, whereas in the other it was attached. The $c_p$ measured at $\alpha > \alpha_{s_0}$ was almost constant throughout, except for a slight discontinuity at the step. At $\alpha < \alpha_{s_0}$, the downstream flow enclosed a large bubble extending over 85% of $L_f$ before adhering to the surface near the trailing edge. The minimum $c_p \approx -0.5$ was almost constant over the leading 25% of the bubble length. This implied that the upstream flow accelerated as it approached the flap, and the acceleration was felt at least 300 mm upstream. This acceleration was also measured with hot wires. The favorable pressure gradient approaching the flap shoulder at $\alpha = 29$ deg thinned the boundary layer, particularly the one that was artificially thickened upstream of the test section. The measured $c_p$ distributions were not affected by large differences in the upstream boundary-layer thickness or by differences in the freestream velocity $U_i$ and therefore by Reynolds number. Even the spreading rate of the mixing layer created by separation was not affected by either parameter.

To provide a simple assessment of the state of the flow, the pressure distributions at each $\alpha$ were integrated, and the data are

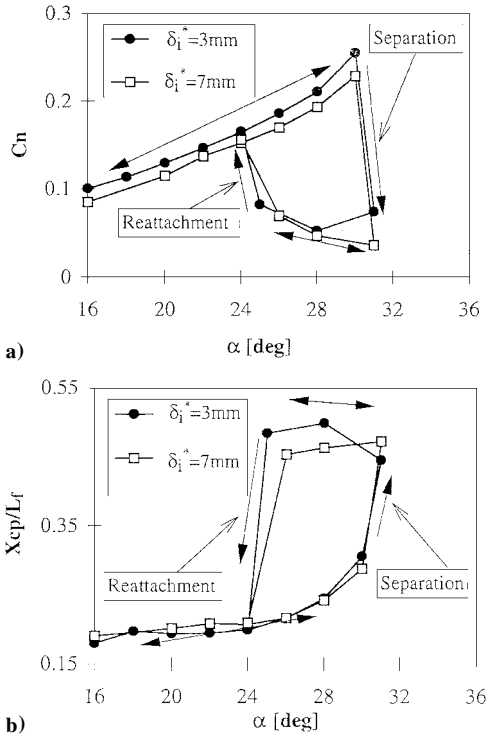


**Fig. 6 a) Dependence of the normal force acting on the flap on $\alpha$ and b) location of the center of pressure as a function of $\alpha$: $F^+ = 0$, $Re = 450 \times 10^3$, $L_f = 740$ mm, and $G/L_f = 0.8\%$.**

presented in terms of a normal force coefficient $c_n$ (Fig. 6a). Another, perhaps more sensitive, parameter is the location of the center of pressure, $x_{cp} = c_{mh}/c_n$, which is almost a constant ($x_{cp}/L_f \approx 0.2$) independent of $\alpha$, provided $\alpha < \alpha_{r_0}$ (Fig. 6b). The sequence at which the data were accumulated is indicated by arrows on both figures in view of the differences between the detachment and reattachment angles. An increase in $\alpha$ beyond $\alpha = \alpha_{r_0} = 24$ deg resulted in a concomitant increase in the size of the bubble, which was manifested by an increase in $c_n$ and a slight move of $x_{cp}$ to the rear of the flap. At $\alpha = 30$ deg and just before separation of the flow, $x_{cp}$ was located near $0.3L_f$. Detachment was marked by a sharp drop in $c_n$ and a discontinuous jump in $x_{cp}$ to the center of the flap. Neither the angle of separation nor that of reattachment was affected by the thickness of the upstream boundary layer that was also altered as shown in Fig. 6. Changing the upstream Reynolds number through a change of velocity did not affect the process either. The insensitivity to Reynolds number is demonstrated by the mean pressure distribution along the flap, which collapses onto a single curve at all values of Reynolds number measured.

Shortening the flap from 740 to 320 mm enabled examination of the effect of $L_f$ on the flow, either directly or through its dependence on Reynolds number. The results proved to be independent of Reynolds number, but they accentuated the significance of the height of the discontinuity $G$ at the flap's leading edge. The angles at which separation or reattachment occurred are very sensitive to $G$, in spite of the fact that the ratio $G/L_f$ was generally smaller than 1% (Fig. 7). For example, a reduction of $G/L_f$ from 1 to 0.6% resulted in an increase of $\alpha_{s_0}$ from 21 to 30 deg, while at the same time increasing the hysteresis angle ($\alpha_{s_0} - \alpha_{r_0}$) from approximately 1 to 5 deg. The observations made on the unperturbed base flow indicate the following.

1) The primary variable determining the flow condition at otherwise identical geometry is $\alpha$, and the crossover from attached to separated flow and vice versa involves hysteresis in $\alpha$.

2) The reattachment and separation angles are sensitive to $G/L_f$ at the leading edge of the flap.

3) The separation and reattachment of the flow are insensitive to the upstream $\delta_i^*$ and to Reynolds number.

4) The mean velocity distribution in the mixing layer surrounding a bubble is similar to the mean flow observed in the classical mixing layer evolving between two parallel streams.

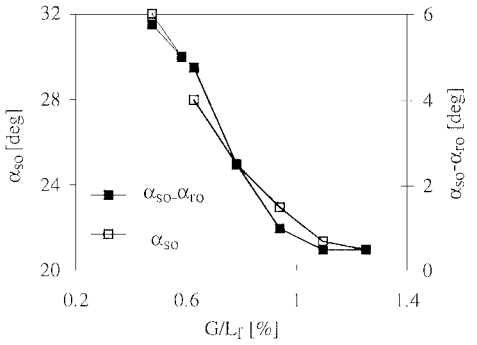


**Fig. 7 Dependence of $\alpha_{s_0}$ and the hysteresis loop ($\alpha_{s_0} - \alpha_{r_0}$) on the relative step height: $Re = 300 \times 10^3$ and $F^+ = 0$.**

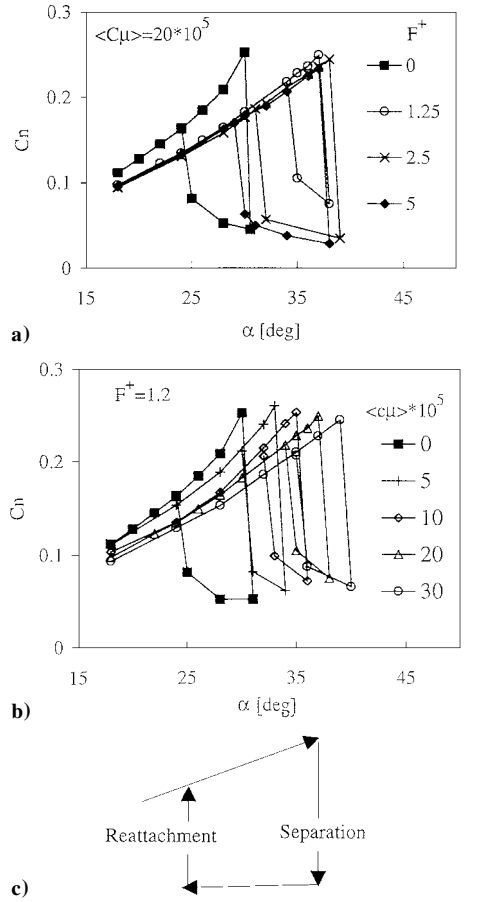


**Fig. 8 Dependence of the normal force on a) $F^+$ and $\alpha$ at $\langle c_\mu \rangle = 20 \times 10^{-5}$ and b) $\langle c_\mu \rangle$ and $\alpha$ at $F^+ = 1.2$: $Re = 450 \times 10^3$, $G/L_f = 0.6$, and $L_f = 740$ mm.**

### B. General Behavior of the Flow Under Active Control

The dependence of $c_n$ on $\alpha$ and on $F^+$ is shown in Fig. 8a for a constant $\langle c_\mu \rangle = 20 \times 10^{-5}$, whereas its dependence on $\langle c_\mu \rangle$ at $F^+ = 1.2$ is plotted in Fig. 8b. Both figures also contain the base flow that might be regarded as a limiting case corresponding to $F^+ = 0$ in Fig. 8a or to $\langle c_\mu \rangle = 0$ in Fig. 8b. All measurements began at a low flap deflection at which the unperturbed flow was attached. After the periodic perturbations were applied, the flap deflection was gradually increased until the flow separated at $\alpha = \alpha_s$. Separation was accompanied by an abrupt decrease in the flap loading.

A gradual decrease in the deflection angle resulted in reattachment at $\alpha = \alpha_r$, which was smaller than the separation angle $\alpha_s$ as shown in the schematic sketch of the process (Fig. 8c). Active excitation increased the separation and the reattachment angles, making $\alpha_s > \alpha_{s_0}$ and $\alpha_r > \alpha_{r_0}$. The maximum difference ($\alpha_s - \alpha_{s_0} = 8$ deg) occurred when $F^+ = 2.5$, whereas the largest difference between $\alpha_r$ and $\alpha_{r_0}$ was 10 deg and corresponded to $F^+ = 1.25$. The increase in the intensity of forcing resulted in a corresponding increase in $\alpha_s$ and $\alpha_r$, which attained $\alpha_s = 40$ deg at $\langle c_\mu \rangle = 30 \times 10^{-5}$.

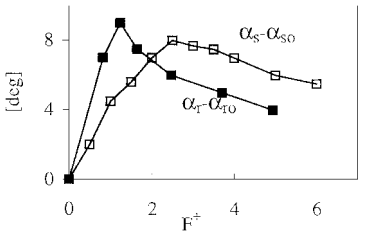


a) $\langle c_\mu \rangle = 20^{-5}$ and $Re = 450 \times 10^3$

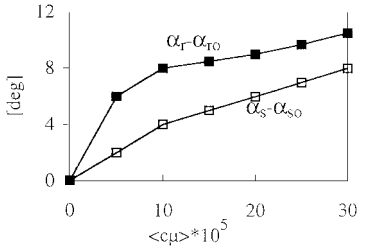


b) $F^+ = 1.2$ and $Re = 450 \times 10^3$

**Fig. 9 Dependence of the separation and reattachment angles on $F^+$ and $\langle c_\mu \rangle$ relative to their natural state.**

The dependence of $(\alpha_s - \alpha_{s_0})$ and of $(\alpha_r - \alpha_{r_0})$ on $F^+$ and on $\langle c_\mu \rangle$ may be observed in Fig. 9. It is clear that the frequencies corresponding to the most effective achievement of reattachment are lower than the frequencies at which separation is most effectively prevented while increasing the flap deflection (Fig. 9a). Also, the range of frequencies at which separation might be prevented at a given $\langle c_\mu \rangle$ and $\alpha$ is broader than the range at which the flow might be forced to reattach. Both $(\alpha_s - \alpha_{s_0})$ and $(\alpha_r - \alpha_{r_0})$ increased with increasing $\langle c_\mu \rangle$ within the range of amplitudes used (Fig. 9b); therefore saturation of the control mechanism was not achieved at the maximum deflection angle of 40 deg attainable in the present experimental setup. Both $\alpha_s$ and $\alpha_r$ increased linearly with increasing $\langle c_\mu \rangle$, provided the latter exceeded $10^{-4}$ in this case.

One may investigate the effects of frequency on $c_n$ at a given geometry and $\langle c_\mu \rangle$ with the objective of determining the most effective $F^+$ for enforcing reattachment or for delaying separation at these conditions, i.e., at a given $\alpha$, $L_f$, and $\langle c_\mu \rangle$ (Fig. 10). The maximum value of $c_n$ attained before separation is $c_n \approx 0.24$ (see Fig. 8); however, it dropped to approximately 0.05 after the flow had completely detached itself from the surface. These values of $c_n$ were independent of $\alpha$. The introduction of oscillations having $\langle c_\mu \rangle \geq 10 \times 10^{-5}$ at $(\alpha - \alpha_{s_0}) = 1.5$ deg increased $c_n$ from 0.05 to $\approx 0.22$ (Fig. 10a). The frequency at which this increase occurred was sensitive to $\langle c_\mu \rangle$. At the highest $\langle c_\mu \rangle$ a jump in $c_n$ was observed at the lowest frequency used, i.e., at $F^+ = 0.4$, but at $\langle c_\mu \rangle = 10 \times 10^{-5}$ it occurred only at $F^+ = 1.25$. After reattachment, the value of $c_n$ decreased very slightly with increasing $F^+$ due to a reduction in the size of the bubble enclosed by the reattaching flow. Repeating the experiment while maintaining $F^+$ constant and increasing $\langle c_\mu \rangle$ from zero to its maximum prescribed value, as noted in Fig. 10b, accentuated the preference of the reattachment process for $F^+ \approx 1.2$. An increase in the maximum $\langle c_\mu \rangle$ level made the frequency band at which reattachment occurred broader; consequently, when $\langle c_\mu \rangle = 30 \times 10^{-5}$, the flow remained attached at $0.4 < F^+ < 2.5$. The dependence of airfoil performance on the frequency of excitation was weak provided the latter was within the range of $0.3 < F^+ < 1.5$ (Ref. 1), while all other parameters were kept constant. These results are consistent with the present observations. It transpired that flow reattachment was more sensitive to the selected value of $F^+$ than flow separation, e.g., while at $\langle c_\mu \rangle = 10 \times 10^{-5}$, the flow that reattached at $F^+ = 1.2$ did not separate as long as $F^+ < 8$; it required a $\langle c_\mu \rangle = 30 \times 10^{-5}$ to reattach it between $F^+ = 0.5$ and 2.5. Thus control effectiveness is sensitive to the initial state of the flow, i.e., whether it is separated.

### C. Parameters Affecting Flow Reattachment

Upon realizing that reattachment of separated flow can be induced by periodic oscillations, the following optimization procedure was initiated.

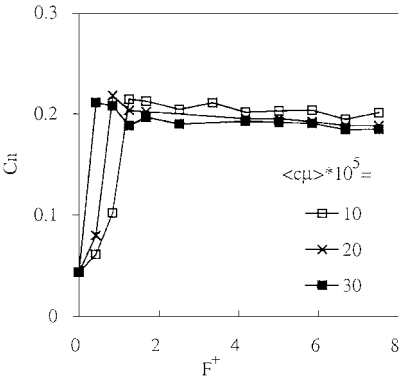


a) Frequency scan

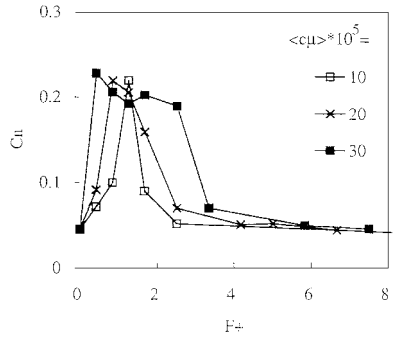


b) Amplitude scan

**Fig. 10 Dependence of $c_n$ on the initial flow conditions at a given $\langle c_\mu \rangle$ or at a given $F^+$: $Re = 450 \times 10^3$, $L_f = 740$ mm, $G/L_f = 0.6\%$, and $\alpha - \alpha_{r_0} = 8$ deg.**

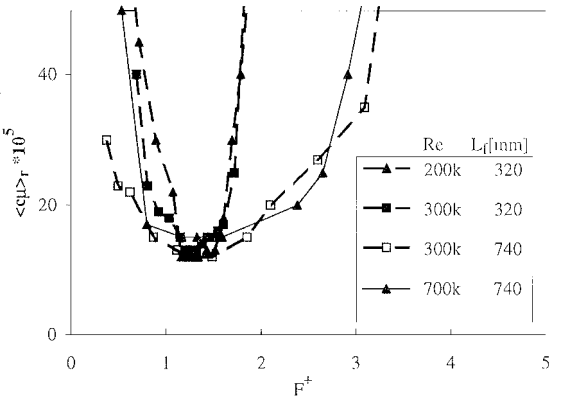


**Fig. 11 Dependence of the minimum momentum coefficient $\langle c_\mu \rangle_r$ required to force reattachment) on $F^+$ and on additional parameters such as Reynolds number or $L_f$: minimum $\langle c_\mu \rangle$ required for reattachment, $\alpha - \alpha_{r_0} = 8$ deg.**

1) The flap deflection was increased beyond $\alpha_{s_0}$, whereupon separation was observed.

2) Active control of the flow at a given $F^+$ was initiated.

3) The intensity of the imposed fluctuations was gradually increased until the flow reattached at some threshold value of $\langle c_\mu \rangle = \langle c_\mu \rangle_r$.

At the optimum frequency, the flow reattached to the surface at lowest $\langle c_\mu \rangle$.

The accuracy at which $\langle c_\mu \rangle_r$ can be determined is probably no better than 20% because the flow on the verge of reattachment is extremely sensitive to extraneous, uncontrolled perturbations, e.g., building vibrations, noise level, etc. Therefore, each experiment was repeated a number of times, but the waiting time for establishing reattachment was limited to 3 min. The reattachment process itself was abrupt and irreversible; however, after reattachment, the flow was very stable, and the level of perturbations could be significantly reduced.

The dependence of $\langle c_\mu \rangle_r$ on $F^+$ is shown in Fig. 11 for various Reynolds numbers, for two flap lengths $L_f = 740$ and 320 mm, and

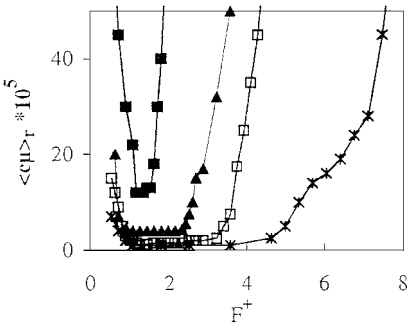


**Fig. 12 Dependence of $\langle c_\mu \rangle_r$ on $F^+$ for various $(\alpha_r - \alpha_{r_0})$: ✱, 1 deg; □, 4 deg; ▲, 6 deg; and ■, 10 deg. $L_f$ = 320 mm, $Re = 200 \times 10^3$–$300 \times 10^3$, $G/L_f$ = 1%, and $\alpha_{r_0}$ = 20 deg.**

for two different values of $\alpha$ that correspond to almost identical values of $(\alpha - \alpha_{r_0}) \approx 9$ deg. The optimum frequency for reattachment is approximately $1.2 < F^+ < 1.5$, and the minimum $\langle c_\mu \rangle_r \approx 12 \times 10^{-5}$. The shorter flap required a much more precise determination of the optimum frequency than the longer one. The results were independent of Reynolds number provided $Re > 2 \times 10^5$. Thickening of the upstream boundary layer had no effect on $\langle c_\mu \rangle_r$, but the increase in the height of the geometrical discontinuity $G$ did.[8] When $G/L_f = 0.01$, $\langle c_\mu \rangle_{at} \approx 12 \times 10^{-5}$, whereas doubling $G/L_f$ resulted in doubling the $\langle c_\mu \rangle$ required for reattachment.

The inclination of the shorter flap (Fig. 12) had a major effect on the minimum value of $\langle c_\mu \rangle$ required for reattachment, $\langle c_\mu \rangle_r$. Whereas at $(\alpha - \alpha_{r_0}) = 1$ deg, $\langle c_\mu \rangle_r \approx 1 \times 10^{-5}$, it increased to $\langle c_\mu \rangle_r \approx 5 \times 10^{-5}$ at 6 deg and to $\langle c_\mu \rangle_r \approx 13 \times 10^{-5}$ at 10 deg. This represents an increase of an order of magnitude in $\langle c_\mu \rangle$ for a change of $\alpha = 8$ deg. The optimum frequency band at which the flow reattaches broadens significantly with decreasing $(\alpha - \alpha_{r_0})$. Whereas at $(\alpha - \alpha_{r_0}) = 8$ deg, the range of effective $F^+$ was small $(1.3 < F^+ < 1.6)$, it increased to $1.2 < F^+ < 4$ at $(\alpha - \alpha_{r_0}) = 1$ deg; nevertheless, the optimum $F^+$ for reattachment remained around $F^+ = 1.3$ regardless of the deflection angle. The broad frequency band at which reattachment is observed at small $(\alpha - \alpha_{r_0})$ is attributed to the inherent sensitivity of the flow to the level of ambient disturbances that might be of amplitude comparable to $\langle c_\mu \rangle_r$.

To understand the cause for reattachment and for the preferred frequency of $F^+ \approx 1$, the velocity in the mixing layer was measured while the flow was excited at low levels insufficient to force reattachment at any frequency. The mean velocity profiles were integrated[8] to provide a measure for the spreading angle of the flow in terms of $(d\theta/dx)$. These data revealed that the mixing layer was thickest opposite the trailing edge of the flap when $F^+ \approx 1$ and the product $(f \cdot \theta / U_\infty) \approx 0.035$. This roughly corresponds to the location at which the mixing layer ceases to spread[6] and where the mean flow becomes neutrally stable to the imposed harmonic perturbations. Frequencies on either side of $F^+ = 1$ proved to be less effective; the lower frequencies did not complete their amplification cycle by the time the perturbations arrived in the vicinity of the trailing edge, whereas the higher ones started to decay much too early. Indeed, the local axial component of the total unsteady momentum coefficient $(c_\mu)'_x$ (due to forcing and turbulence) attained its highest value at the trailing edge when $F^+ = 1$. In this case $(c_\mu)'_x$ had undergone an amplification by an order of magnitude between $x/L_f = 0.2$ and 1. Power spectra indicated[8] that the amplitude of all of the frequencies whose $F^+ < 1$ increased with increasing $x$, as also happened in the canonical mixing layer. When the shear layer was excited at $F^+ = 2$, the frequencies in the neighborhood of the excitation frequency started to decay at $x/L_f = 0.5$. The amplitude distributions of the phase-locked, streamwise velocity fluctuations filtered at the forcing frequency resemble the amplitudes measured by Gaster et al.[9] in the forced mixing layer. When the forcing frequency corresponded to $F^+ = 1$, the amplitude distribution was very similar to the calculated neutrally stable mode (Fig. 13). This gives the criterion for the optimum periodic forcing, which generates a mode that becomes neutrally stable at the trailing edge of the flap. Such a mode extracted most of its energy from the flow and therefore required the smallest input $\langle c_\mu \rangle_r$ necessary to cause reattachment.

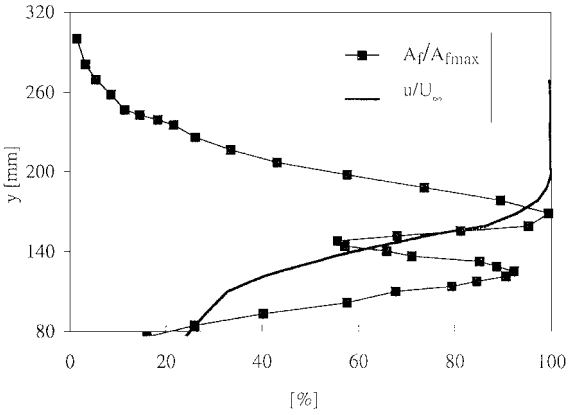


**Fig. 13 Mean velocity profile and amplitude distribution of the streamwise component of the velocity perturbation in the mixing layer opposite the trailing edge of the flap. The forcing frequency corresponds to $F^+ = 1$: separated flow at $Re = 200 \times 10^3$, $F^+ = 1$, $\langle c_\mu \rangle = 10^{-5}$, and $\alpha - \alpha_{s_0} = 8$ deg.**

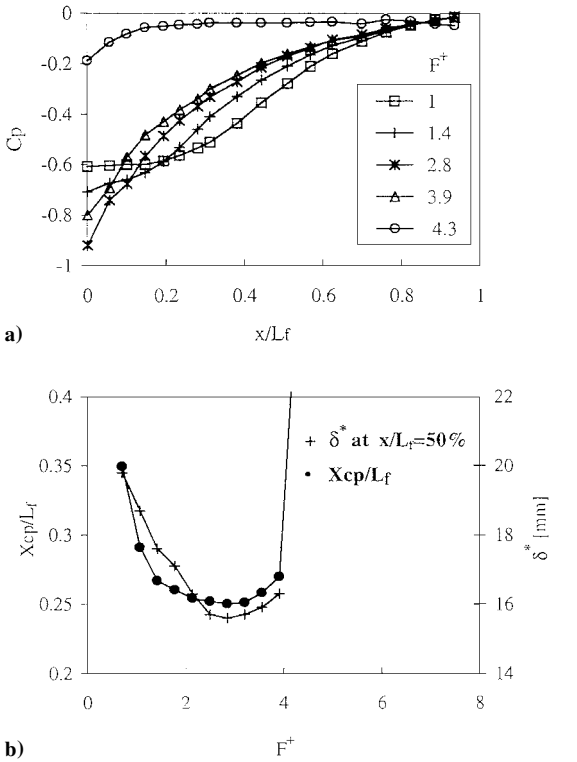


**Fig. 14 a) Pressure distribution over the flap after a forced reattachment at various values of $F^+$ and b) location of the center of pressure over the flap and the thickness of the boundary layer at midflap location as functions of $F^+$: $\langle c_\mu \rangle = 20 \times 10^{-5}$, $\alpha = 25$ deg, $\alpha - \alpha_{s_0} = 5$ deg, $L_f$ = 320 mm, $G/L_f$ = 1%, and $Re = 200 \times 10^3$.**

### D. Parameters Determining the Delay of Separation

The pressure distribution realized on the flap after a forced reattachment of the flow at optimum $F^+$ (Fig. 14a) is similar to the pressure distribution observed before separation in the absence of forcing (see Fig. 4). It occurs, however, at smaller $\alpha$. The effect of separation or reattachment on the upstream flow is no less significant than on the pressure distribution over the flap, even without excitation (see Fig. 5). This implies that reattachment of separated flow, or vice versa, represents a change of state both upstream and downstream of the separation location. It is also a process in which hysteresis is unavoidable.

In the absence of external excitation, the state of the flow is determined uniquely by the size of the bubble that also provides a criterion for the impending separation. The addition of periodic forcing adds new degrees of freedom requiring additional criteria to define the state of the flow because a burst of a bubble is no longer the sole

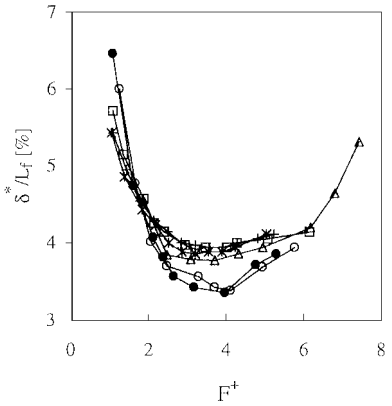


**Fig. 15 Dependence of $\delta^*/L_f$, measured at 40% of $L_f$, on $F^+$: $x/L_f$ = 40% and $\langle c_\mu \rangle = 10^{-5}$. *Re* and $L_f$ (mm) are given, respectively, as □, 120 and 320; |, 200 and 320; ✕, 300 and 320; △, 300 and 740; ○, 450 and 740; and ●, 700 and 740.**

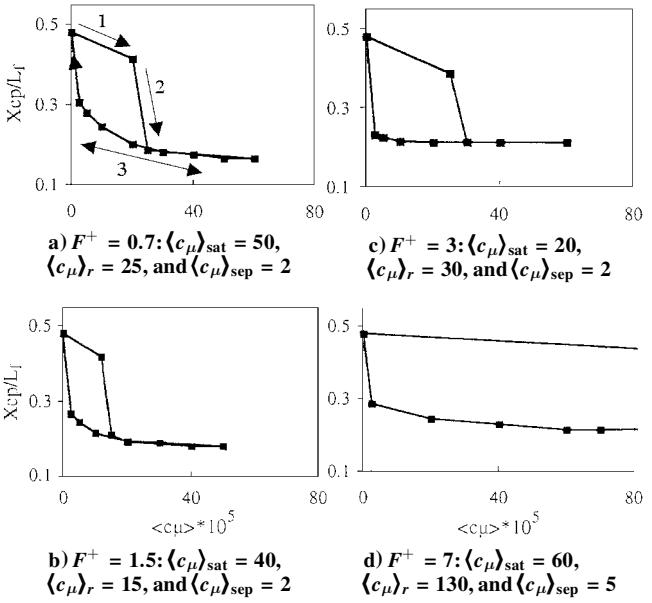


**Fig. 16 Dependence of the hysteresis loop in $x_{cp}$ on $F^+$ and on $\langle c_\mu \rangle$: $\alpha$ = 32 deg and $\alpha - \alpha_{s_0}$ = 1.5 deg.**

mode of separation. Separation at high $F^+$ (Fig. 10b) may not involve a bubble at all, as it may be initiated from the trailing edge, whereas a small bubble located near the leading edge is not affecting the process. Consequently the effectiveness of the excitation may be measured either by the location of the center of pressure or by local boundary-layer parameters, e.g., skin friction, shape factor, or $\delta^*$, reflecting on the ability of the flow to withstand the adverse pressure gradient.

The effect of the excitation frequency on the pressure distribution over the shorter flap ($L_f = 320$ mm) may be deduced from Fig. 14a. In this experiment $\langle c_\mu \rangle = 20 \times 10^{-5}$ while $F^+$ ranged from 1 to 4.3. There was a very large bubble when $F^+ = 1$, which shrank with increasing $F^+$ and seemed to disappear around $F^+ = 2.8$. Increasing the forcing frequency resulted initially in a small reduction in $c_p$, to be followed by separation initiated from the trailing edge until it covered most of the flap. The center of pressure (Fig. 14b) moved upstream when $F^+$ was increased between $0.7 < F^+ < 2$, it remained around its minimum value while $2 < F^+ < 3.2$, and it crept downstream before the occurrence of separation around $F^+ = 4$. The forcing frequency had to be reduced to $F^+ = 2.8$ before reattachment was realized. Thus, the control of separation and reattachment by changing the excitation frequency contains another form of hysteresis. The displacement thickness measured at the center of the flap tracked the movement of the center of pressure (Fig. 14b), suggesting that the most effective forcing for separation delay was around $F^+ = 2.8$. Although the center of pressure and $\delta^*$ were continuously monitored, only one criterion will be discussed in conjunction with any variable.

The dependence of $\delta^*/L_f$ on $F^+$ is plotted in Fig. 15 for the two flaps used and for a variety of Reynolds numbers. Large differences in Reynolds number had little effect on the dimensional value of $\delta^*$ measured on a given flap because the mechanism responsible for most of the turbulence production is inviscid and is associated with the inflection point in the mean velocity profile. Separation did not take place on the longer flap up to $F^+ < 8$. One should note that the values of $(\alpha - \alpha_{s_0}) \approx 1.5$ deg for both flaps and the dimensional value of the step height $G$ were identical. In both cases the most effective forcing frequencies, i.e., those that thinned $\delta^*$ the most, were between $3 < F^+ < 4$. Neither the increase in $G$ nor that in $(\alpha - \alpha_{s_0})$ had any significant effect on the optimum values of $F^+$ used in delaying separation. An increase in either factor, however, reduced the $F^+$ at which separation occurred and increased the minimum value of $\delta^*$ measured at a prescribed location on the flap. However, provided $F_s^+ > 4$, then the most effective frequencies to delay separation remain unchanged, i.e., $3 < F^+ < 4$. The value of $\delta^*_{\min}$ increased almost linearly with either $G$ or $(\alpha - \alpha_{s_0})$; thus the effect of either variable on the flow is similar. An increase in $\langle c_\mu \rangle$ did not change the most effective $F^+$ but rather increased $F_s^+$. It appears that increasing $\langle c_\mu \rangle$ above a certain threshold level led to saturation and ineffectiveness. Thus, the most effective prevention of separation by oscillatory means occurs at $3 < F^+ < 4$, provided the available $\langle c_\mu \rangle$ is adequate.

Changing $\langle c_\mu \rangle$ while keeping all other parameters constant also affects the flow over the flap. The dependence of $x_{cp}$ on $\langle c_\mu \rangle$ is plotted in Fig. 16. At $(\alpha - \alpha_{s_0}) = 1.5$ deg, the flow is naturally separated, and it remains in this condition while $\langle c_\mu \rangle$ is carefully increased (arrow 1) until it exceeds a threshold value (arrow 2) and the flow reattaches. After reattachment one may reduce $\langle c_\mu \rangle$ and increase the size of the bubble or increase $\langle c_\mu \rangle$ and reduce it even further. The process is entirely reversible (arrow 3) unless $\langle c_\mu \rangle$ is reduced below $2 \times 10^{-5}$, resulting in separation. Separation and reattachment due solely to changes in $\langle c_\mu \rangle$ also contain a hysteresis loop. The ratio between $\langle c_\mu \rangle_r / \langle c_\mu \rangle_s \approx 12.5$ when forcing at $F^+ = 0.7$ (Fig. 16a). The decrease in the bubble size with increasing $\langle c_\mu \rangle$ results in an upstream movement of $x_{cp}$. The dependence of $\delta^*$ (measured at $x/L_f = 0.5$) on $\langle c_\mu \rangle$ decreased asymptotically with increasing $\langle c_\mu \rangle$ after reattachment occurred. It is entirely saturated at $\langle c_\mu \rangle_{sat} \approx 50 \times 10^{-5}$ (Fig. 16a) or at $\langle c_\mu \rangle_{sat} \approx 20 \times 10^{-5}$ (Fig. 16c). The saturation amplitude and the thickness of the boundary layer at saturation $\delta^*_{sat}$ were determined for a variety of Reynolds numbers, $G$, and $L_f$, and for $(\alpha - \alpha_{s_0})$.

It is interesting to note that the minimum $\langle c_\mu \rangle$ needed to maintain the flow attached was approximately constant, independent of $F^+$. The accuracy at which $\langle c_\mu \rangle_s$ can be determined is low because it is close to the resolution limit of the experiment, i.e., $\langle c_\mu \rangle_s = 2 \times 10^{-5}$. It is clear that the size of the hysteresis loop describing the forces and moments acting on the flap as a function of $\langle c_\mu \rangle$ is dominated by the $\langle c_\mu \rangle$ required for reattachment (Fig. 16). The smallest hysteresis loop corresponds to $\langle c_\mu \rangle_r / \langle c_\mu \rangle_s \approx 7.5$ and occurs at $F^+ = 1.5$ (Fig. 16b). Repeating the experiment at $F^+ = 7$ required an order of magnitude larger $\langle c_\mu \rangle$ to close the loop (Fig. 16d). The minimum values of $\langle c_\mu \rangle_{sat}$ (mentioned in the labels of Figs. 16a–16d) correspond to $F^+ = 3$ and not to the value of $F^+$ controlling the size of the hysteresis loop. The minimum value of $\delta^*_{sat}$ was also realized at $F^+ = 3$.

The pressure distribution over the flap when the amplitude of the imposed perturbations was decreased to the minimum level necessary to keep the flow attached, i.e., $\langle c_\mu \rangle_s \approx 10^{-5}$, was very sensitive to $F^+$. Two limiting cases are shown in Fig. 17. At $F^+ = 0.7$, the reduction in amplitude generated a bubble whose dimensions were commensurate with the length of the flap. Thus, a small additional increase in the bubble length caused it to burst. In this case the flow is already separated over most of the flap in spite of the large $c_n$ it generated. At $F^+ = 7$ the size of the bubble was insignificant ($d^2 c_p / dx^2 = 0$ at $x/L_f < 0.1$; Fig. 17), but the boundary layer at the trailing edge was thick and depleted from momentum. Thus a reduction in $\langle c_\mu \rangle$ caused the separation to propagate from the trailing edge upstream.

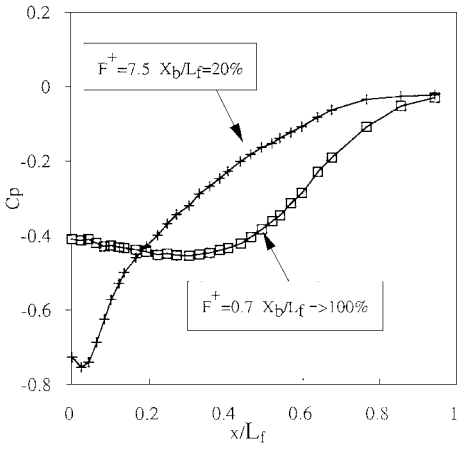


**Fig. 17 Pressure distribution over the flap on the verge of separation at $F^+ = 7.5$ and 0.7: $\langle c_\mu \rangle_{sep} + 10^{-5}$, $Re = 450 \times 10^3$, $L_f = 740$ mm, and $\alpha - \alpha_{s_0} = 1.5$ deg.**

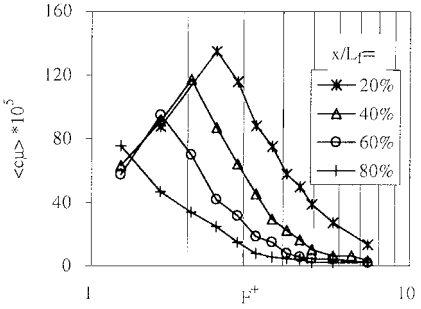


**Fig. 18 Amplification and decay of the local $\langle c_\mu \rangle_x$, measured at four locations along the flap, with $F^+$: $Re = 450 \times 10^3$, $\langle c_\mu \rangle = 20 \times 10^{-5}$, $\alpha - \alpha_{s_0} = 1.5$ deg, $L_f = 740$ mm, and $G/L_f = 0.5\%$.**

The amplification and decay of the phase-locked oscillations in the direction of streaming are assessed by measuring the local

$$\langle c_\mu \rangle_x = \frac{1}{L_f U_i^2} \int_{y=0}^{\infty} [\langle u'(x) \rangle]^2 \, dy \qquad (4)$$

for various forcing frequencies at a constant input amplitude of $\langle c_\mu \rangle = 20 \times 10^{-5}$ (Fig. 18). At $x/L_f = 0.2$, the perturbations corresponding to $F^+ = 2.5$ had undergone the highest amplification of almost sevenfold. Perturbations at other frequencies on either side of $F^+ = 2.5$ were amplified less, and perturbations at $F^+ > 6.5$ did not even sustain their original value of $20 \times 10^{-5}$ by the time they propagated to $x/L_f = 0.2$. The frequency corresponding to the most-amplified wave decreased with increasing distance from the leading edge and dropped below $F^+ = 1.2$ at $x/L_f = 0.8$. The decay of $\langle c_\mu \rangle_x$ with increasing $F^+$ is exponential. It appears, therefore, that the strategies for delaying separation by periodic perturbations have two conflicting requirements: 1) a need for high frequency to reduce the size of the bubble and 2) a need for maintaining a minimum threshold value of $\langle c_\mu \rangle_x$ at the trailing edge.

Excessive $\langle c_\mu \rangle_x$ at the trailing edge is a waste that could be diverted either to increase $\alpha$ or to reduce the size of the bubble and hence to improve the overall pressure recovery. One may infer from Fig. 18 that an input of $\langle c_\mu \rangle = 20 \times 10^{-5}$ and $3 < F^+ < 4$ decays at the trailing edge by an order of magnitude and that suffices to prevent separation (Fig. 16). A reduction in the frequency below a threshold $F^+$ may cause a bubble to burst and lead to separation from the leading edge. An increase in $F^+$ beyond a prescribed threshold may result in separation being initiated at the trailing edge and creeping upstream with increasing $F^+$.

The dependence of $\langle c_\mu \rangle_x$ on $(f^* x/U_\chi)$ is shown in Fig. 19 as it reinforces the notion that the dominant amplification process in the flow surrounding a bubble is inviscid and similar to the one observed in the plane turbulent mixing layer. Forcing the flow at various frequencies $F^+$ generated perturbations whose maximum amplitude was attained at $(f^* x/U_\chi) = 1$, where the flow becomes neutrally stable at a streamwise distance $x = (U_\chi/f)$ as it does in

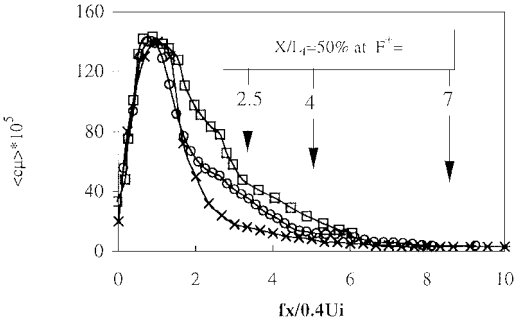


**Fig. 19 Variation of the local $\langle c_\mu \rangle_x$ with $(fx/U_i)$ and $F^+$; the arrows point to the locations at which $X/L_f = 0.5$: $\langle c_\mu \rangle = 20 \times 10^{-5}$, $Re = 450 \times 10^3$, $\alpha - \alpha_{s_0} = 1.5$ deg, $L_f = 740$ mm, and $G/L_f = 0.5\%$. $F^+$: □, 2.5; ○, 4; and ×, 7.**

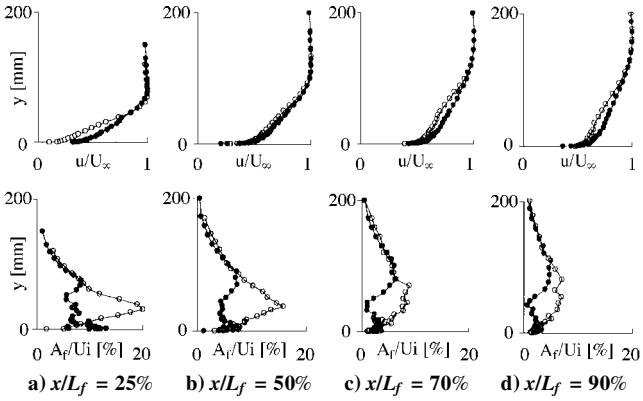


**Fig. 20 Effect of $F^+$ on the mean velocity profiles and on the amplitude distributions at four locations along the flap. Attached flow: $L_f = 740$ mm, $\alpha = 29$ deg, $\langle c_\mu \rangle = 20 \times 10^{-5}$, and $Re = 450 \times 10^3$; ○, $F^+ = 1.2$, and ●, $F^+ = 2.5$.**

the canonical mixing layer.[4,5] However, whereas a representative phase velocity in the mixing layer is the average velocity of the two streams participating in the mixing process $[U_\chi = 0.5(U_1 + U_2)]$, a representative phase velocity in the present flow is lower ($U_\chi = 0.4U_i$, where $U_i$ corresponds to $U_1$, and whereas $U_2$ is assumed to vanish). It is possible that $U_\chi$ is affected by the reverse flow inside the bubble requiring that $U_2 < 0$ or by the adverse $(dp/dx)$. The maximum amplitude attained and the amplification rate of $\langle c_\mu \rangle_x$ with $(fx/U_\chi)$ were independent of $F^+$, whereas the spatial rate of decay of $\langle c_\mu \rangle_x$ at $(fx/U_\chi) > 1$ was not (Fig. 19). Arrows marking the location of the midchord point are drawn on Fig. 19 to help the reader identify the amplitude prevailing at various streamwise locations. Only at $F^+ \approx 2.5$ is there still some significant $\langle c_\mu \rangle_x$ left near the trailing edge of the flap.

Mean velocity profiles and normalized amplitude distributions representing data collected at four streamwise locations and two forcing frequencies are plotted in Fig. 20. The measurements were carried out at $\alpha < \alpha_{s_0}$, and thus, in the absence of excitation, there was a large bubble over the flap. The mean velocity profiles were easily distorted by the imposed excitation. Higher frequency of forcing increased the skin friction at the wall and made the velocity profiles fuller, i.e., changed the traditional integral parameters used in boundary-layer analysis. Forcing at $F^+ = 2.5$ was more effective in transporting momentum to the surface and reducing the mean strain $(dU/dy)$ over most of the boundary layer with the exception of the wall region. The large $(dU/dy)$ accompanying $F^+ = 2.5$ near the surface results in a high intensity of $u'$ observed in this region. The production of velocity fluctuations at $F^+ = 1.2$ is in the outer region, and it is stimulated by an inviscid instability associated with the inflection point in the mean flow. Thus the maximum amplitude of the fundamental frequency coincides with the location at which $d^2\bar{U}/dy^2 = 0$ (Fig. 20). The turbulence intensity near the surface is negligible when the flow is forced at $F^+ = 1.2$, whereas it is very high at $F^+ = 2.5$. An inert surface layer was also encountered in the Stratford ramp experiment representing a boundary layer, which is

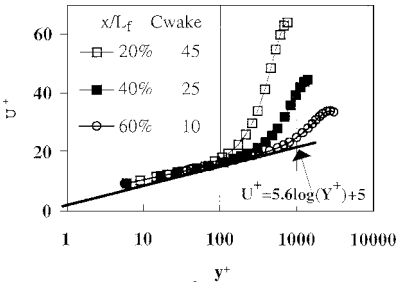


**Fig. 21a Reduction in the wake component of the velocity profile with increasing distance in the direction of streaming: $\alpha - \alpha_{s_0} = 2$ deg, $F^+ = 3, \langle c_\mu \rangle = 30E-5$, and $Re = 450 \times 10^3$.**

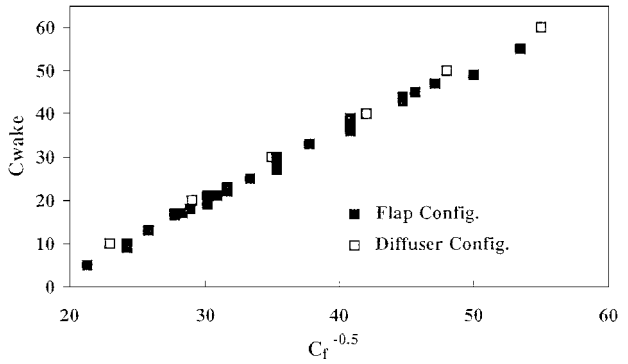


**Fig. 21b Unique dependence of the wake-component constant on the skin-friction coefficient and its independence from all other parameters considered: $F^+ = 1$–$8, \langle c_\mu \rangle \times 10^5 = 10$–$100, x/L_f = 20\%$–$80\%$, $Re = 200 \times 10^3$–$700 \times 10^3, \alpha - \alpha_s = 1$–$8$ deg, $Ui = 6$–$14$ m/s, and $L_f = 320$–$740$ mm.**

constantly maintained on the verge of separation.[10] It is interesting to note that forcing at different frequencies did not alter the boundary-layer thickness (Fig. 20). This is in clear distinction to the effects of excitation in free shear flows, which altered the local width of the flow and its rate of spread rather than distorting the form of the mean velocity profile. A dimensional ordinate is retained in Fig. 20 in order not to mask the effects of excitation on the velocity distributions.

The imposed two-dimensional perturbations increase the spanwise coherence of the large structures controlling the flow. The spanwise extent of these eddies was assessed by measuring the cross spectra of the $u'$ fluctuations at various separation distances $\Delta z$ and calculating the coherence and the phase from the data. The plots obtained are similar to those in the forced turbulent wall jet,[11] suggesting that the effect of two-dimensional forcing is significant near the solid surface. The phase scrambling at all frequencies lower than the frequency of forcing was also suppressed by the excitation.

When the mean velocity profiles are plotted in the wall coordinates (Fig. 21a), the universal logarithmic distribution, i.e., $U^+ = A \log(y^+) + B$), remains unchanged regardless of the forcing frequency or $\langle c_\mu \rangle$. The maximum value of $y^+$ fitting the universal logarithmic distribution depends not only on $\alpha$ and on $x$, i.e., on the pressure gradient, but also on the parameters representing the excitation. It can be best correlated with the dependence of the shape factor $H$ on these parameters. The general representation of the law of the wake also applies in all cases considered,[2] i.e., $W = C \sin^2(\pi y/2\delta)$, where the constant $C$ depends on $x$, $\alpha$, $\langle c_\mu \rangle$, and $F^+$. The constant representing the wake component in the mean velocity profile correlates well with skin friction. In fact, $C \propto (C_f)^{-0.5}$ regardless of all of the aforementioned parameters (Fig. 21b). Furthermore, a similar experiment performed in a diffuser yielded identical results, which are also plotted.

### E. Some Effects Associated with Steady Blowing

Steady blowing through the slot provides a benchmark for proving the efficacy of the present method because blowing is still used to control separation. For example, a steady $c_\mu$ of $200 \times 10^{-5}$ was required to get the flow to reattach (Fig. 22), whereas reattachment by forced oscillations was attained by $\langle c_\mu \rangle = 12 \times 10^{-5}$ at

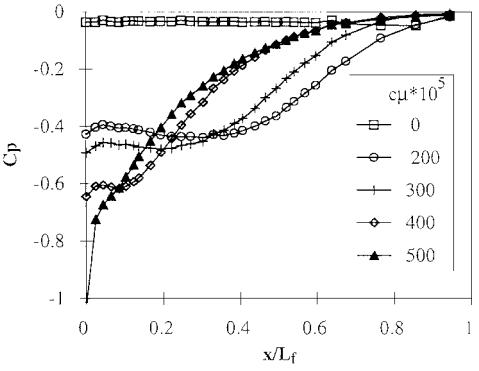


**Fig. 22 Effect of steady blowing on the pressure distribution over the flap in the absence of periodic perturbations: $F^+ = 0$, $Re = 450 \times 10^3$, $L_f = 740$ mm, $G/L_f = 0.5\%$, and $\alpha - \alpha_{s_0} = 2$ deg.**

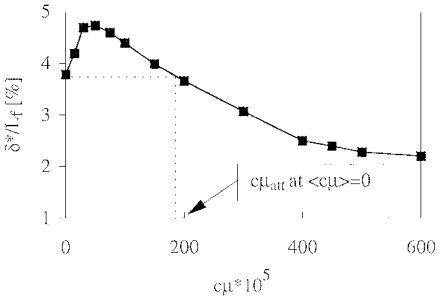


**Fig. 23 Effect of adding steady $c_\mu$ to a prescribed $\langle c_\mu \rangle = 20 \times 10^{-5}$ on the boundary-layer thickness measured at $X/L_f = 0.4$: $F^+ = 2.5, \langle c_\mu \rangle = 20 \times 10^5, Re = 450 \times 10^3, \alpha - \alpha_{s_0} = 2$ deg, $L_f = 740$ mm, and $G/L_f = 0.5\%$.**

$F^+ = 1.5$ (see Fig. 11). To reduce the ensuing bubble by steady blowing required an additional increase in the steady value of $c_\mu$ to $500 \times 10^{-5}$, whereas a simple increase in $F^+$ at the reattachment value of $\langle c_\mu \rangle = 12 \times 10^{-5}$ did better. Reducing slowly the intensity of the blowing resulted in total separation at $c_\mu = 180 \times 10^{-5}$. Steady blowing is therefore very inefficient in controlling reattachment or separation.

Separation was prevented at $F^+ = 3$ at the amazingly low $\langle c_\mu \rangle \approx < 2 \times 10^{-5}$. A combination of steady and oscillatory blowing was not very effective in this case either, because the slot was located at the place where natural separation occurred and there was no need to advect the imposed oscillations farther downstream. For example, a combined $C_\mu = [180; 20] \times 10^{-5}$ is required to achieve, in this case, the same results as the oscillatory blowing alone. Another measure reflecting the state of the flow is the displacement thickness $\delta^*$, which was thinner everywhere when $C_\mu = [0; 20] \times 10^{-5}$ than it was at $C_\mu = [100; 20] \times 10^{-5}$ or when $c_\mu = [400; 0] \times 10^{-5}$. Measuring $\delta^*$ at a single streamwise location for various intensities of combined $C_\mu$ reveals clearly the detrimental effect of the addition of steady blowing, provided $c_\mu < 180 \times 10^{-5}$. Only above this threshold does an increase in $c_\mu$ result in reduction of $\delta^*$ (Fig. 23).

## V. Conclusions

The introduction of two-dimensional, periodic oscillations into a turbulent boundary layer enables it to resist larger adverse pressure gradients without separating. It therefore increases the performance of airfoils at incidence exceeding natural separation. The optimum frequency for reattachment of the flow to a straight surface is at $F^+ = 1$. After reattachment, however, the flow encloses a large bubble that may be reduced by increasing $F^+$. The most effective frequency to prevent separation is around $3 < F^+ < 4$. At high forcing frequencies the flow separates from the trailing edge because $F^+$ is so high that the imposed oscillations dissipate before reaching the end of the flap. Hysteresis between attached and separated conditions is typical to this bistable flow, and it may be induced not only by $\alpha$ (which is a well-known phenomenon at low Reynolds number) but by $F^+$ and $\langle c_\mu \rangle$ as well. Steady blowing at low momentum coefficients was found to be detrimental to this method of separation control.

## Acknowledgments

The project was sponsored in part by a grant from the Research and Development Office of the Israel Ministry of Defense and monitored by A. Kuritzki. The authors wish to thank A. Seifert for his help and useful comments.

## References

[1]Seifert, A., Bachar, T., Koss, D., Shepshelovich, M., and Wygnanski, I., "Oscillatory Blowing: A Tool to Delay Boundary-Layer Separation," *AIAA Journal*, Vol. 31, No. 11, 1993, pp. 2052–2060.

[2]Katz, Y., Nishri, B., and Wygnanski, I., "The Delay of Turbulent Boundary Layer Separation by Oscillatory Active Control," *Physics of Fluids A*, Vol. 1, No. 2, 1989, pp. 179–181.

[3]Collins, F. G., and Zelenevitz, J., "Influence of Sound upon Separated Flow over Wings," *AIAA Journal*, Vol. 13, No. 3, 1975, pp. 408–410.

[4]Seifert, A., Darabi, A., and Wygnanski, I., "Delay of Airfoil Stall by Periodic Excitation," *Journal of Aircraft*, Vol. 33, No. 4, 1996, pp. 691–698.

[5]Oster, D., Wygnanski, I., Dziomba, B., and Fiedler, H., "The Effect of Initial Conditions on the Two-Dimensional, Turbulent Mixing Layer," *Structure and Mechanics of Turbulence*, edited by H. Fiedler, Vol. 75, Lecture Notes in Physics, Springer–Verlag, Berlin, 1978, pp. 48–59.

[6]Oster, D., and Wygnanski, I., "The Forced Mixing Layer Between Parallel Streams," *Journal of Fluid Mechanics*, Vol. 123, 1982, pp. 91–129.

[7]Weisbrot, I., and Wygnanski, I., "On Coherent Structures in a Highly Excited Mixing Layer," *Journal of Fluid Mechanics*, Vol. 195, 1988, pp. 137–159.

[8]Nishri, B., "On the Control of Separation and Reattachment from a Flap," Ph.D. Thesis, Dept. of Fluid Mechanics and Heat Transfer, Tel-Aviv Univ., Ramat-Aviv, Israel, May 1995 (in Hebrew).

[9]Gaster, M., Kit, E., and Wygnanski, I., "Large Scale Structures in a Forced Turbulent Mixing Layer," *Journal of Fluid Mechanics*, Vol. 150, 1985, pp. 23–39.

[10]Ellsbery, K., "The Stratford Ramp," M.S. Thesis, Aerospace and Mechanical Engineering Dept., Univ. of Arizona, Tucson, AZ, 1996.

[11]Katz, Y., Horev, E., and Wygnanski, I., "The Forced Turbulent Wall Jet," *Journal of Fluid Mechanics*, Vol. 242, 1992, pp. 577–609.

R. W. Wlezien
*Associate Editor*